

PAPER • OPEN ACCESS

Mesoscopic interference for metric and curvature & gravitational wave detection

To cite this article: Ryan J Marshman *et al* 2020 *New J. Phys.* **22** 083012

View the [article online](#) for updates and enhancements.

Recent citations

- [Relative acceleration noise mitigation for nanocrystal matter-wave interferometry: Applications to entangling masses via quantum gravity](#)
Marko Toroš *et al*
- [Realization of a complete Stern-Gerlach interferometer: Toward a test of quantum gravity](#)
Yair Margalit *et al*
- [Small-Sized Interferometer with Fabry–Perot Resonators for Gravitational Wave Detection](#)
Nikolai Petrov and Vladislav Pustovoi



PAPER

Mesoscopic interference for metric and curvature & gravitational wave detection

OPEN ACCESS

RECEIVED

13 December 2019

REVISED

21 May 2020

ACCEPTED FOR PUBLICATION

23 June 2020



PUBLISHED

6 August 2020

Original content from
this work may be used
under the terms of the
[Creative Commons
Attribution 4.0 licence](#).

Any further distribution
of this work must
maintain attribution to
the author(s) and the
title of the work, journal
citation and DOI.



Ryan J Marshman^{1,4} , Anupam Mazumdar² , Gavin W Morley³, Peter F Barker¹,
Steven Hoekstra² and Sougato Bose¹

¹ Department of Physics and Astronomy, University College London, Gower Street, WC1E 6BT London, United Kingdom

² Van Swinderen Institute, University of Groningen, 9747 AG Groningen, The Netherlands

³ Department of Physics, University of Warwick, Gibbet Hill Road, Coventry CV4 7AL, United Kingdom

⁴ Author to whom any correspondence should be addressed.

E-mail: r.marshman.17@ucl.ac.uk

Keywords: Stern–Gerlach interferometry, general relativity, gravitational waves

Abstract

A compact detector for space-time metric and curvature is highly desirable. Here we show that quantum spatial superpositions of mesoscopic objects could be exploited to create such a detector. We propose a specific form for such a detector and analyse how asymmetries in its design allow it to directly couple to the curvature. Moreover, we also find that its non-symmetric construction and the large mass of the interfered objects, enable the detection gravitational waves (GWs). Finally, we discuss how the construction of such a detector is in principle possible with a combination of state of the art techniques while taking into account the known sources of decoherence and noise. To this end, we use Stern–Gerlach interferometry with masses $\sim 10^{-17}$ kg, where the interferometric signal is extracted by measuring spins and show that accelerations as low as $5 \times 10^{-15} \text{ ms}^{-2} \text{ Hz}^{-1/2}$, as well as the frame dragging effects caused by the Earth, could be sensed. The GW sensitivity scales differently from the stray acceleration sensitivity, a unique feature of the proposed interferometer. We identify mitigation mechanisms for the known sources of noise, namely gravity gradient noise, uncertainty principle and electro-magnetic forces and show that it could potentially lead to a metre sized, orientable and vibrational noise (thermal/seismic) resilient detector of mid (ground based) and low (space based) frequency GWs from massive binaries (the predicted regimes are similar to those targeted by atom interferometers and LISA).

1. Introduction

Matter wave interferometry has been very successful with atoms [1], and implemented already with macromolecules (10^4 amu mass) [2]. There has been a push to extend this to larger superpositions, or more macroscopic masses [3–17], or both [18, 19] to explore collapse model modifications of quantum mechanics [20, 21] and to test whether the gravitational field is fundamentally quantum in nature [22, 23]. However, as it will be a considerable effort to realize these interferometers, it is really important to examine their usefulness beyond the purely fundamental and postulated processes. In addition, while searching for applications, it makes sense to be optimistic about the regimes achievable by combining several state-of-the-art quantum technologies and experimental techniques. With the above motivations, here we examine sensor/detector applications of the large mass, large superposition regime [18, 19, 22] in interferometry. We find an application in which such superpositions are used to detect fully the classical gravitational effects in a location as quantified by the metric and curvature. This comes against a backdrop of proposals of smaller particle interferometers [24–26] or larger quantum optomechanical systems [27, 28] to detect a g_{00} metric component, whose variations can be used to infer the associated component of curvature, the direct measurement of such curvature [29] or to detect the Earth's rotation [30, 31] or general relativistic effects [32–35]. The most challenging entities to detect are the gravitational waves (GWs), the g_{ij} metric components, whose detection has been a huge recent success using kilometre long

optical interferometers [36, 37], with future devices proposed in space [38]. On the other hand there are also proposals for usage of atomic interferometers [39–45] and various resonators [46–50], but nothing yet on the potential of interferometers for propagating (untrapped) objects much larger than single atoms.

In this paper, we will discuss how mesoscopic-object interference could be employed for detecting metric and curvature (MIMAC), and moreover present an example scheme based on the Stern–Gerlach principle [18, 51–53, 64]. Thus this paper has three aims: 1. To show that large mass interferometry with a certain asymmetric design would allow the capability to directly detect unprecedented regimes of inertial and gravitational effects with compact sized devices, 2. To present an explicit example interferometer and demonstrate how to, in general, infer the signals it can sense 3. Present a viability study for this specific interferometer to highlight that these regimes will soon be accessible. Here it noteworthy that there could be other, perhaps more viable schemes based on other methods to prepare superpositions of mesoscopic objects. Such investigations would be fuelled by our findings under aims 1 and 2.

In the particular type of interferometer which we study as an example model, although a spatial interferometry involving superpositions of separated motional states takes place, the output signal of the interferometer is encoded in a spin degree of freedom in a manner which is insensitive to the initial noise in the motional state (thermal and seismic). We demonstrate that it can be used to observe the metric and, as a result of using a non-symmetric set-up, also ‘directly’ observe the derivatives in the interferometric signal which determine the curvature of a perturbed Minkowski metric (as opposed to indirectly inferring the curvature by measuring the metric in nearby locations and then approximating derivatives of the metric). It is due to this ability to directly sense curvature through the interferometer that we describe the interferometer as sensitive to metric *and* curvature (cf section 4). Additionally, these interferometers enable the measuring of the Earth’s frame dragging and gravitational waves of certain strength and frequency range. In all these cases, it is remarkable, and indeed directly due to the high masses of the objects undergoing interferometry, that the interferometer is very compact (one meter or smaller), and highly sensitive at a single object level, i.e., does not require a high flux of objects.

This paper will proceed as follows: section 2 will review the general form of the action for a mass moving through non-trivial space-time in the non-relativistic limit. It also presents the standard arguments in favour of using larger ‘mesoscopic’ masses as the interferometric particles. Of course the observations of this section are independent of the specific type of mesoscopic object interferometer that one uses, and as such is adaptable to other future proposals. Section 3 presents a specific proposal for a mesoscopic object interferometer for detecting the space-time metric and its curvature (MIMAC). This interferometer employs Stern–Gerlach interferometry and is a modified version of the previously proposed interferometer suggested in other contexts with both atoms [51–53] and mesoscopic particles [18, 22]. Section 4 will present the exact components of the space-time metric detectable by the suggested form of MIMAC in such a way to also provide a guide to analyse future interferometer proposals. Sections 5–7 will present and discuss how the most interesting signals found in section 4, namely Newtonian gravity and its associated curvature, frame dragging and gravitational waves (GW), can be detected. This will include suggesting the basic experimental parameters required for detection and presenting the resulting sensitivities. Finally section 8 will discuss in detail the requirements for the most challenging of the signals, gravitational wave observation in the mid-band frequency and demonstrate how, although ambitious, such a device does not appear to be beyond realisability. This is done by presenting how current state-of-the-art techniques match or beat the minimum experimental requirements for theoretical gravitational wave observation. We also discuss the primary expected noise sources and their effects in such a device, namely decoherence effects, gravity gradient noise (GGN), the Heisenberg uncertainty limit and electro-magnetic effects. While section 2 points out the potential of a new regime and section 3 is presents a necessary modification of an existing apparatus, sections 5–7 are entirely new theoretical results. Section 8 is, of course, compiling state-of-art commercially available equipment and experimental achievements by various laboratories to justify the potential realisability of our scheme.

2. Non-relativistic action

The signal extracted by an interferometer coupled to the space-time metric is the phase difference ($\Delta\phi$) between the two arms of the interferometer. This is given by $\Delta\phi = \Delta S/\hbar$, where ΔS is the difference in action between the two paths through the interferometer. As such, relative to any classical gravimeter or similar classical experiment, this $1/\hbar$ dependence in the final phase will hugely amplify the final measured signal in a quantum interferometer. If we consider the space-time metric, $g_{\mu\nu}$, as slightly perturbed, as is true for Earth based measurements, the space-time metric can be written as $g_{\mu\nu} = \eta_{\mu\nu} + h_{\mu\nu}$ where $\eta_{\mu\nu}$ is the standard Minkowski metric with signature $(-+++)$ and $h_{\mu\nu}$ is some small perturbation that may have

space and time dependencies. We will also take the non-relativistic limit for the interferometric particles motion, as a result the laboratory time t can be taken to be approximately equivalent to the proper time. Then the action for a particle of mass m travelling along a trajectory ι in the is

$$\begin{aligned} S &= -mc \int_{\iota} ds \\ &= -mc \int_{\iota} \sqrt{ds^2} \\ &= -mc \int_{\iota} \left(g_{\mu\nu} \frac{dx^\mu}{d\tau} \frac{dx^\nu}{d\tau} \right)^{1/2} d\tau \\ &= mc^2 \int_{\iota} \left[-(\eta_{00} + h_{00}) \frac{dt^2}{d\tau^2} - h_{0j} \frac{v^j}{c} \frac{dt}{d\tau} - h_{i0} \frac{v^i}{c} \frac{dt}{d\tau} - (\delta_{ij} + h_{ij}) \frac{v^i v^j}{c^2} \right]^{1/2} d\tau \end{aligned} \quad (1)$$

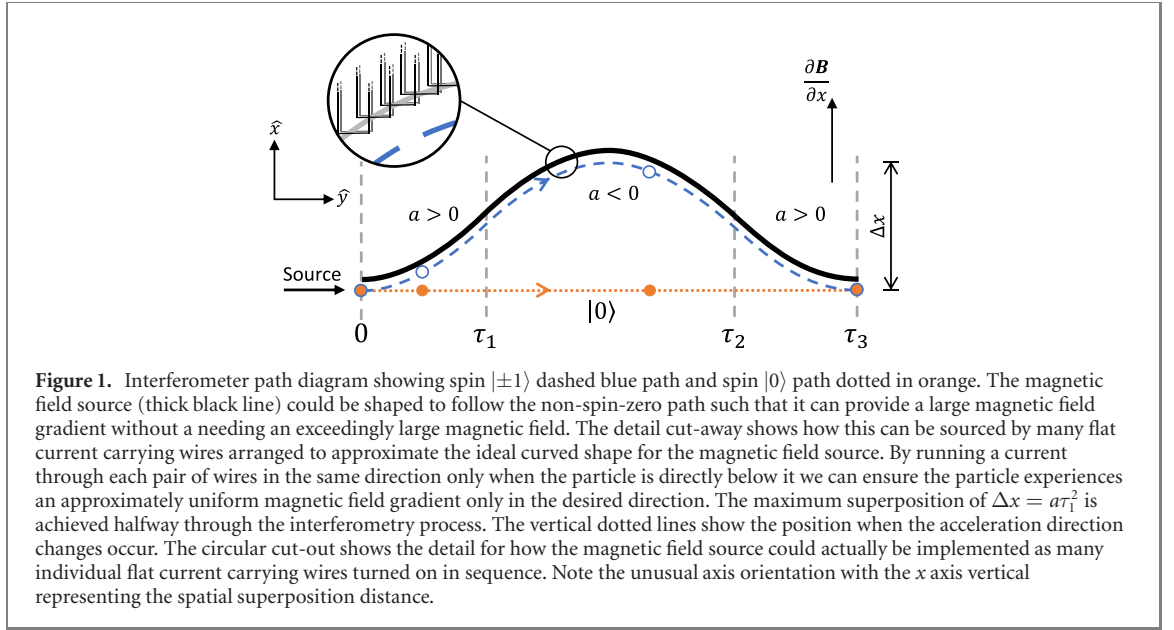
$$\approx m \int_{\iota} \left[c^2 \left(1 - \frac{h_{00}}{2} \right) - ch_{0j} v^j - (\delta_{ij} + h_{ij}) \frac{v^i v^j}{2} \right] dt, \quad (2)$$

where δ_{ij} is the Kronecker delta. From the above formula it is evident that compared to the h_{00} component (Newtonian potential), the terms h_{0j} (frame dragging) are harder to detect as c is replaced by a non-relativistic velocity v_j , while h_{ij} (Gravitational Waves) will be the most difficult to detect with c^2 replaced by $v_i v_j$. On the other hand, a high value of m (compared to atomic masses) are expected to increase the sensitivity to all terms, potentially allowing the detection of signals which would otherwise be too small to see. For example, for similar velocities and times (we will show how to achieve this in later sections), when one uses nano-objects of mass 10^{-17} kgs, there is an $O(10^8)$ times amplification in the final signal ($\Delta\phi$) compared to a heavy atom.

3. Interferometric setup

Here we will present an example form for a mesoscopic object interferometer. This proposal amounts to a modification of the devices previously proposed for atomic and mesoscopic interferometry. Stern–Gerlach interferometry of the type we are proposing to use requires a spin embedded in a nano-crystal. This is a very generic requirement and the proposal does not rely on a specific type of spin system or crystalline host. The primary requirement is that a superposition of embedded spin states remains coherent for the duration of an experiment, which is a common requirement in the field of quantum computing with spin qubits. For the moment, consider a mesoscopic mass (nano-meter sized crystal) containing an embedded spin 1 degree of freedom (three spin states $|+1\rangle, |0\rangle, |-1\rangle$). One example is a diamond crystal of nanometer scale diameter with a nitrogen-vacancy (NV) centre spin, which is generally considered as a promising candidate for similar experiments [10, 12, 54, 55]. Another example is a rare-earth dopant spin in a crystal [56, 57]. The mass is initially optically trapped, made neutrally charged [58] and rapidly cooled [59–63]. The internal spin state is then initialised by the application of a sudden microwave pulse in a superposition of spin eigenstates $\frac{1}{\sqrt{2}}(|+1\rangle + |0\rangle)$. At this point ($t = 0$) the mass is released from the trap in a motional wavepacket $|\psi(0)\rangle$ centred at velocity $\mathbf{v} = (0, v_y, 0)$ with the aforementioned internal spin superposition. The presence of a magnetic field gradient ($\partial_x \mathbf{B}$) in the x direction induces an acceleration $\mathbf{a} = (a, 0, 0)$ on the $|+1\rangle$ spin state. The magnetic field gradient source we consider here consists of many flat carbon nanotubes arranged as shown in the detailed cut-out of figure 1. To ensure a uniform magnetic field gradient is achieved the current through the wire can be switched on only when it is directly above the particle. This acts to generate the spatial superposition required while also coupling the spin and motional states. The acceleration of the non-zero spin component is reversed at time $t = \tau_1$ and again at $t = \tau_2 = 3\tau_1$ by reversing the spin state, while the acceleration magnitude is maintained so that at any time t , the combined spin and motional state is $\frac{1}{\sqrt{2}}(|0\rangle |\psi_0(t)\rangle + |\sigma\rangle |\psi_\sigma(t)\rangle)$, where σ represents the non-zero spin state. This procedure will lead to the maximum spatial superposition distance Δx occurring at time $t = 2\tau_1$, at which point the centres of the spatial states $|\psi_0(2\tau_1)\rangle$ and $|\psi_\sigma(2\tau_1)\rangle$ are separated by $\Delta x = a\tau_1^2$. These are then brought back together so that their motional states exactly overlap at time $t = \tau_3 = 4\tau_1$, i.e., $|\psi_0(4\tau_1)\rangle = |\psi_\sigma(4\tau_1)\rangle$.

This spin-motion coupled interferometry has two striking consequences [18]: (i) The relative phase $\Delta\phi$ between the interferometric arms is mapped on to the spin state in the form $\frac{1}{2}e^{i\phi_0(t)} ((e^{i\Delta\phi_s} - 1) |0\rangle + (e^{i\Delta\phi_s} + 1) |\uparrow\rangle)$, so that it can be measured by measuring the spin state alone. For example, by measuring the probability of the state to be brought to the spin state $|0\rangle$ after the application of a third microwave pulse. (ii) The $\Delta\phi$ depends solely on the difference between phases



accumulated in the interferometric paths, and is quite independent of $|\psi(0)\rangle$ making the interferometric signal unaffected by an initial mixed thermal state or other noise (e.g. seismic) which occurs prior to the initialising microwave pulse, which can always be modelled as probabilistic choices of $|\psi(0)\rangle$. Any phase difference $\Delta\phi \geq \frac{1}{\sqrt{N}}$ will then be detectable after N measurements.

Thus the whole interferometric process will lead to the state of the particles state evolving approximately as

$$\begin{aligned}
 \text{Initial state:} & & & & |0\rangle \otimes |\psi(0)\rangle \\
 \text{Microwave pulse:} & & & & \frac{1}{\sqrt{2}} (|0\rangle + |\sigma\rangle) |\psi(0)\rangle \\
 \text{Spatial superposition created} \\
 \text{and maintained for time } t: & & & & \frac{1}{\sqrt{2}} (e^{i\phi_0(t)} |0\rangle |\psi_0(t)\rangle + e^{i\phi_\sigma(t)} |\sigma\rangle |\psi_\sigma(t)\rangle) \\
 \text{Spatial wavefunctions} \\
 \text{brought to overlap:} & & & & \frac{1}{\sqrt{2}} (e^{i\phi_0(t)} |0\rangle + e^{i\phi_\sigma(t)} |\sigma\rangle) |\psi(t)\rangle \\
 \text{Microwave pulse:} & & & & \frac{1}{2} ((e^{i\phi_\sigma(t)} - e^{i\phi_0(t)}) |0\rangle + (e^{i\phi_\sigma(t)} + e^{i\phi_0(t)}) |\sigma\rangle) |\psi(t)\rangle \\
 \text{Final state:} & & & & \frac{1}{2} e^{i\phi_0(t)} ((e^{i\Delta\phi_S} - 1) |0\rangle + (e^{i\Delta\phi_S} + 1) |\sigma\rangle) |\psi(t)\rangle \quad (3)
 \end{aligned}$$

Here $|\psi(t)\rangle$ is the original spatial state of the particle if it were to freely evolve and evaluated at time t , $|\psi_0(t)\rangle$ and $|\psi_\sigma(t)\rangle$ are the mass state in the spin-zero and non-zero arms of the interferometer respectively and $|0\rangle$ and $|\sigma\rangle$ are the respective spin states. This is an approximation of the evolution undertaken by the particle, whereby each effect is taken to occur stepwise. The magnetic field gradient state creates and recombines the spatial superposition, the microwave pulses create and recombines the spin superpositions. Of particular note is that the initial state of the mass factors in the final result, this will trivially hold in general, even if more complex states, for example thermal states, are used as the initial state.

This interferometric system amounts to an asymmetric modification of that proposed by Wan *et al* [18]. For a more in depth discussion of the required parameters required to realise the most sensitive and ambitious form of the interferometer we will propose can be seen in section 8.

4. Observable components of space-time metric

To determine which components of the metric perturbation $h_{\mu\nu}$ are observable, we expand the action, S , to the second order in derivatives of $h_{\mu\nu}$ assuming a temporally static and spatially slowly varying metric.

Specifically we take

$$h_{\mu\nu}(x, y, t) \approx h_{\mu\nu}(0, 0, 0) + x(t)\partial_x h_{\mu\nu}(0, 0, 0) + y(t)\partial_y h_{\mu\nu}(0, 0, 0) + \frac{1}{2!} (x(t)^2 \partial_x^2 h_{\mu\nu}(0, 0, 0) + y(t)^2 \partial_y^2 h_{\mu\nu}(0, 0, 0) + 2x(t)y(t)\partial_x \partial_y h_{\mu\nu}(0, 0, 0)) \quad (4)$$

For clarity we will from now write $h_{\mu\nu}(0, 0, 0)$ as $h_{\mu\nu}$. This gives the difference in the action between the two interferometric paths due to the different components $h_{\mu\nu}$ ($\mu, \nu = 0, x, y, z$) as

$$\begin{aligned} \Delta S(h_{00}) &= mc^2 a \tau_1^3 \left(\partial_x h_{00} + \frac{23}{60} a \tau_1^2 \partial_x \partial_x h_{00} + 2v_y \tau_1 \partial_x \partial_y h_{00} \right) \\ &= mc^2 a \tau_1^3 \left(\partial_x h_{00} + \frac{23}{60} a \tau_1^2 \partial_x \partial_x h_{00} + \dots \right), \end{aligned} \quad (5)$$

$$\begin{aligned} \sum_j \Delta S(h_{0j}) &= mcav_y \left(2\tau_1^3 (\partial_x h_{0y} - \partial_y h_{0x}) + 4v_y \tau_1^4 (\partial_y \partial_y h_{0x} - \partial_x \partial_y h_{0y}) + \frac{23}{30} a \tau_1^5 (\partial_x \partial_x h_{0y} - \partial_x \partial_y h_{0x}) \right) \\ &= mcav_y \left(-2\tau_1^3 \partial_y h_{0x} + 2\tau_1^3 \partial_x h_{0y} + \frac{23}{30} a \tau_1^5 \partial_x \partial_x h_{0y} + \dots \right), \end{aligned} \quad (6)$$

$$\begin{aligned} \Delta S(h_{xx}) &= -\frac{2}{3} ma^2 \tau_1^3 \left(h_{xx} + 2v_y \tau_1 \partial_y h_{xx} + \frac{1}{2} a \tau_1^2 \partial_x h_{xx} + \frac{51}{20} v_y^2 \tau_1^2 \partial_y^2 h_{xx} + \frac{43}{280} a^2 \tau_1^4 \partial_x^2 h_{xx} \right) \\ \Delta S(h_{xy}) &= mav_y^2 \tau_1^3 \partial_y h_{xy} + 2mav_y^3 \tau_1^4 \partial_y^2 h_{xy} + \frac{293}{60} ma^2 v_y^2 \tau_1^5 h_{xy} \\ \Delta S(h_{yy}) &= -mav_y^2 \tau_1^3 \partial_x h_{yy} - \frac{38}{3} mav_y^3 \tau_1^4 \partial_x \partial_y h_{yy} - \frac{23}{60} ma^2 v_y^2 \tau_1^5 \partial_x^2 h_{yy} \end{aligned} \quad (7)$$

$$\sum_{i,j} \Delta S(h_{ij}) = \frac{-2}{3} h_{xx} ma^2 \tau_1^3 + \dots = \frac{-2}{3} h_{xx} mv_x^2 \tau_1 + \dots$$

The equations presented here are split such that, once truncated, they correspond to the Newtonian potential (equation (5)), frame dragging (equation (6)) and Gravitational waves (equation (7)) effects. Here we note that the example interferometer can directly detect certain components of the metric perturbation. Specifically the term h_{xx} and, as rotating the apparatus is equivalent to relabelling the spatial direction, the spatial components of the metric in general. Furthermore as the action is directly dependent on the second derivatives of $h_{\mu\nu}$, such an apparatus would also be sensitive to the local space-time curvature⁵. This allows the experimentalist to simply identify certain components of the Riemann tensor $R_{\mu\nu\sigma\rho}$ in the above equations term by term, it is for this reason we consider the interferometer directly sensitive to space-time curvature. The role of the asymmetry in the interferometer can also now be seen from 7, given the second order terms $a^2 \tau_1^2 \approx (v_x)^2$ dependence, asymmetry is necessary to generate an action difference between the arms. For example, if a symmetric interferometer was used, by taking the initial spin state of $\frac{1}{\sqrt{2}}(|+1\rangle + |-1\rangle)$, then both arms would contain the same v_x^2 dependent phase as seen in equation (7). These would cancel in the final phase difference, leaving the interferometer no longer sensitive to GWs.

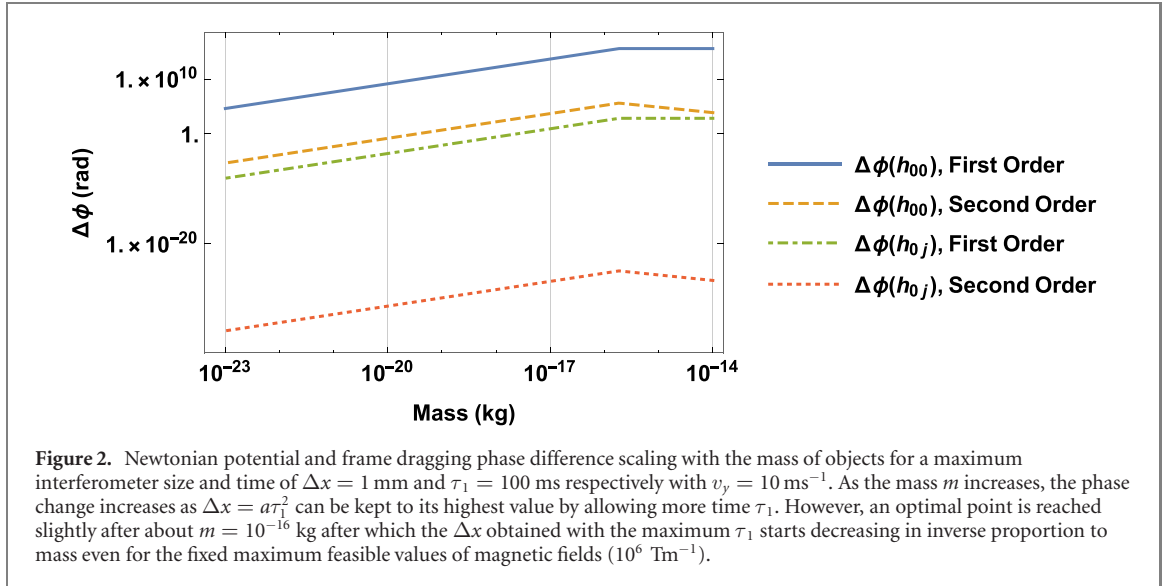
In the following sections we will explore the basic experimental considerations for detecting Newtonian gravity and its associated curvature (section 5), frame dragging effects (section 6) and gravitational waves (section 7). We present the exact form that the signals will take, discuss their predicted amplitudes to discern how well they can be detected and for the case of the Newtonian potential, we will also explore and characterise a variety of different sources which could be generating the signal.

5. Newtonian potential

Considering only the first non-Minkowski term in 2 we can make the standard substitution for the Newtonian potential, $h_{00} = 2MG/c^2 R$. We define the vertical as the x -axis, the experiment taken to be performed at ground level so R is radius of the Earth, and M Earth's mass, the difference in action between the two arms up to the second order in $(a\tau_1^2/R)$ is

$$\Delta S(h_{00}) \approx -\frac{2mMG}{R^2} a \tau_1^3 + \frac{23mMG}{15R^3} a^2 \tau_1^5, \quad (8)$$

⁵ The complete curvature is characterised by the Riemann tensor which is defined by $R_{\mu\nu\sigma\rho} = \frac{1}{2}(\partial_\sigma \partial_\mu h_{\rho\nu} + \partial_\nu \partial_\rho h_{\mu\sigma} - \partial_\nu \partial_\mu h_{\rho\sigma} - \partial_\sigma \partial_\rho h_{\mu\nu})$.



$$\Delta\phi(h_{00}) \approx -2 \times 10^{35} \text{ kg}^{-1} \text{ m}^{-1} \text{ s}^{-1} \times m a \tau_1^3 + 2 \times 10^{28} \text{ kg}^{-1} \text{ m}^{-2} \text{ s}^{-1} \times m a^2 \tau_1^5. \quad (9)$$

This is consistent with the notion that any curvature detection will be of the form $U(L/R)^2$ where U is the gravitational potential and L is the characteristic laboratory length (in the above case, $L \sim a\tau_1^2$) [65]. Despite this quadratic suppression, it is still detectable due to the $1/\hbar$ factor in the phase difference. As such, we can expect to observe even second order effects (curvature effects) as large phase shifts. Figure 2 shows how these results scale with the mass of the object in the interferometer assuming a maximum allowed value of the spatial separation ($a\tau_1^2$). From figure 2 it can be seen that a mass of 10^{-16} kg in a ~ 1 mm interferometer with integration time $\tau_1 \sim 100$ ms gives a detection of acceleration with sensitivity down to $\sim 5 \times 10^{-15}$ ms $^{-2}$ Hz $^{-1/2}$. This result is for the case of sending a single particle through the interferometer at a time and as such represents a lower bound on the sensitivity of such a detector. This compares favourably with the recent work demonstrating the direct detection of metric curvature of a test mass with a sensitivity of 5×10^{-9} ms $^{-2}$ Hz $^{-1/2}$ [29].

This detector could also be used to detect smaller masses and more local signals. For example, the mass M at distance R which yields a detectable phase shift compared to it not being there, effectively it ceasing to exist, is given by

$$M = \frac{\hbar R^2}{2\sqrt{N}mG\Delta x\tau_1} \quad (10)$$

which suggests for the interferometer specifications used for figure 2, at a distance of 1 km, a mass of approximately 4 kg is detectable provided the mass has moved from a very far distance to this 1 km range or by varying the interferometer orientation relative to the mass. On the other hand, all stationary masses naturally present around the interferometer will not act as a noise when detecting other signals as they will provide a constant phase difference between arms for a fixed orientation of the interferometer.

We can also consider detecting the motion of a mass. Taking the motion to be slow enough that the interferometer phase can be found for the mass M at R before it moves a distance d and detected again. The minimum movement detectable will then be

$$d \approx \frac{\hbar R^3}{4\sqrt{N}mMG\Delta x\tau_1} \quad (11)$$

where it has been assumed that $d \ll R$. For example the previous $M = 4$ kg mass a distance $R = 100$ m away will produce a detectable phase variation if it moves by $d \approx 0.5$ m or more. This can act as a noise source when looking to detect other signals, this will be discussed below in section 8.

6. Frame dragging

To explore the detection of frame dragging, the ‘frame dragging’ metric given in [66] was considered. Written in spherical with ψ the azimuthal and θ the polar angles:

$$ds^2 = -H(r) c^2 dt^2 + J(r) [dr^2 + r^2 d\theta^2 + r^2 \sin^2(\theta) (d\psi - \Omega dt)^2] \quad (12)$$

where

$$H(r) \approx 1 - \frac{8GM}{c^2 r} + \dots, \quad J(r) \approx 1 + \frac{8MG}{c^2 r} + \dots, \quad (13)$$

where the binomial expansion approximation has been used for being in the linearized limit, and $\Omega = 2MG\nu/c^2 R$ is the scaled angular velocity of the central rotating mass, where once again M is the mass of the Earth, R is its radius and ν is its angular velocity. The relevant component of 12 is the cross term $d\psi dt$.

The apparatus is taken to be aligned parallel with the equator and surface of the Earth, and taking a small angle approximation with regards to the angular distance the mass travels along the interferometer in the 'y' direction measured from the centre of the Earth. Defining M as the mass of the Earth, R its radius, and ν its angular velocity gives a phase difference, again to the second order in $(a\tau_1^2/R)$

$$\Delta\phi(h_{0j}) \approx \frac{8mMG\nu \sin^2(\theta) a v_y}{\hbar c^2 R} \left(\tau_1^3 - \frac{3M^2 G^2}{c^4 R^2} \tau_1^3 \right) + \frac{92mM^3 G^3 \nu \sin^2(\theta) v_y}{5\hbar c^6 R^4} a^2 \tau_1^5. \quad (14)$$

Substituting all known constants, assuming the interferometer is located on the surface of the Earth, gives $\Delta\phi(h_{0j}) \approx 4 \times 10^{21} m a v_y \tau_1^3$ as the first order, metric dependent phase and $\Delta\phi(h_{0j}) \approx 6 \times 10^{-4} m a^2 v_y \tau_1^5$ for the second order, curvature dependent phase. These effects are significantly more modest so high precision measurements would be needed, specifically to measure the second order term. Such measurements would provide an independent verification of the results from gravity probe B [33]. Figure 2 also shows the phase due to first and second order effects independently with respect to the object mass.

7. Gravitational waves

Our setup can also extract the phase from the transverse traceless perturbations around the Minkowski background:

$$h_{xx} = -h_{yy} = h_+ \cos(\psi_0 + \omega t) \quad (15)$$

$$h_{xy} = h_{yx} = h_\times \cos(\psi_0 + \omega t), \quad (16)$$

where ψ_0 is the GW phase at the interferometer at $t = 0$ in the interferometers reference frame. We have assumed the GW is propagating along the $x_3 = z$ direction perpendicularly to the interferometer with angular frequency ω and taken the two helicity states of the GWs as $h_+, h_\times \ll 1$. We also ignore the kinetic energy component of the atoms action, see 2, as it is not relevant for the purpose of detecting the phase. The GW induced phase difference is

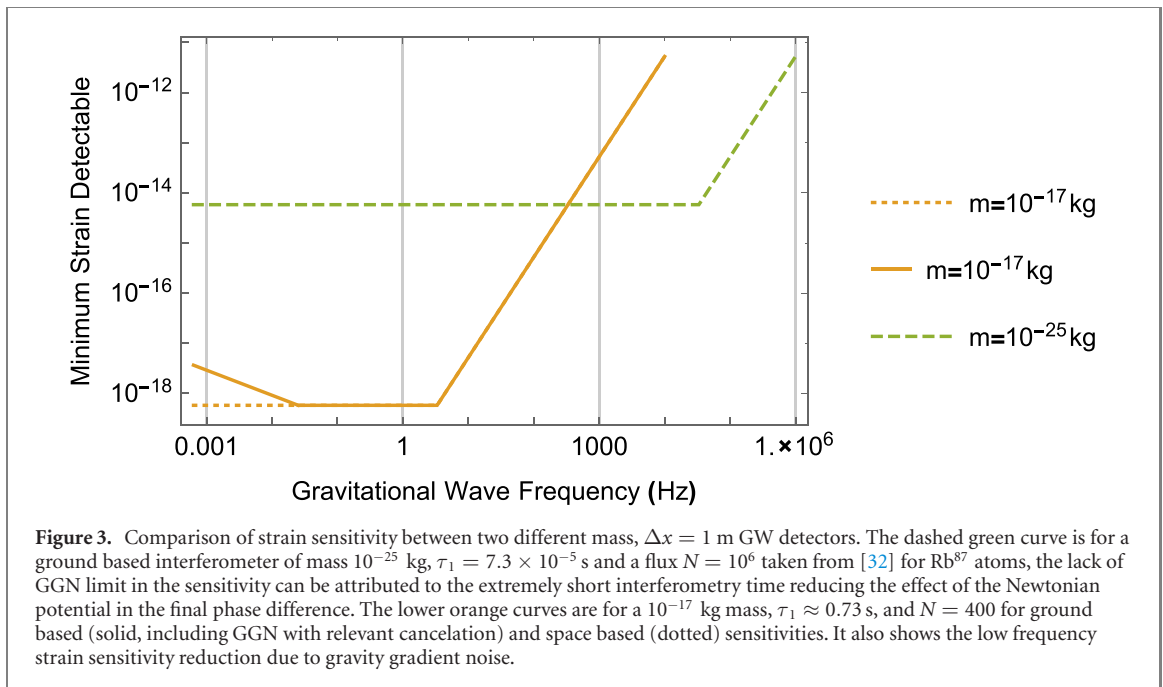
$$\Delta\phi(h_{ij}) = \frac{4mh_+ a^2 \tau_1 \cos(\psi_0) \cos(\omega\tau_1)}{\hbar\omega^2} \left(1 - \frac{\sin(\omega\tau_1)}{\omega\tau_1} \right) \quad (17)$$

$$\approx \frac{2mh_+ a^2 \tau_1^3 \cos(\psi_0)}{3\hbar} \quad (18)$$

where ψ_0 is the wave's phase at $t = 2\tau_1$ and the approximate form holds when $\omega\tau_1 \ll 1$. Note the h_\times component is not recorded in our interferometer, as it is proportional to v_x which varies between positive and negative values, thus cancelling itself out unlike h_+ as it is a function of v_x^2 . A rotated apparatus detects h_\times .

The underlying mechanism for this phase difference is ultimately through the particle coupling to the local space-time parameters (the metric). The metric is what will be directly affected by the GW and this is detected through the phase evolution as given by the action, see 2. Note that our apparatus is *not* directly detecting the tidal acceleration of the particle caused by the GW. In fact, it is negligible compared to that generated by the magnetic field gradient needed to enable the interferometry. It is simply measuring the spatial stretching/contraction as caused by the GW in the same manner as it would measure a permanent change in the relevant components of the metric. Of course there is an unavoidable time variation of the metric due to the GW, but we do not exploit this variation⁶—the time variation of the metric is much slower than an individual run of the interferometer for the frequencies our detector is most sensitive to. Essentially the interferometer detects phase changes due to static metric components. In this way the correct analogy here between laser interferometers and our interferometer is that the mass is the replacement of the

⁶ Here we are specifically referring to the variation during a single particles traversal of the interferometer. The sinusoidal modulation of the phase difference due to the variation of the metric from one run to the next will be how the GW is measured.



photons. They both act to measure the change in spatial distances due to the GW. As the path length difference of $\sim h_+ L$ is essentially being measured in units of the matter wave de Broglie wavelength, $\sim 10^{-17}$ m, $L \sim 1$ m suffices (note in our case $L = \Delta x$). Let us emphasize here that one should *not* interpret our interferometer as detecting the tidal acceleration as given by $h_+ L \omega^2$ directly acting on the mass. This also leads directly to how the GW sensitivity in our interferometer scales uniquely compared to the acceleration sensitivity. Consider increasing the magnetic field gradient applied, such that $a \tau_1^2 = \Delta x$ remains fixed, while reducing τ_1 . The GW induced phase difference scales as $\Delta \phi(h_{ij}) \propto \frac{\Delta x^2}{\tau_1} h_{ij}$ because the GW metric couples to the velocity of the particle ($S \propto h_{ij} v^i v^j$) while the stray acceleration induced phase difference scales as $\Delta \phi(h_{00}) \propto \Delta x \tau_1 h_{00}$. As such the GW sensitivity can be further enhanced while suppressing the noise effects in our signal, giving an improved signal to noise ratio. Thus our interferometer is qualitatively very different from LIGO/LISA. A second *crucial* difference between laser interferometers and MIMAC is that there is no back-action and as such the related standard quantum limit is not a limiting factor. This is because the measurement only occurs *once* after the interferometry has taken place, and the position is not measured either, only the final spin state. Indeed our interferometer is closest in mechanism to single atom interferometers, which were suggested as some of the early atom-interferometry schemes for GW detection [39–41].

These two differences form the basis of the potential future advantages this interferometer holds over laser interferometers, in which the standard quantum limit and Newtonian noise act as the primary limits on the sensitivity. Neither are fundamentally limiting with MIMAC or a MIMAC like interferometer.

With respect to the early atom interferometers, our advantage stems from the much larger m for our interferometers as our Stern–Gerlach (SG) methodology opens up the scope to create a high enough Δx , even with the increased mass. Here we should note that the more advanced proposals from atom interferometry such as atomic GW interferometric sensor (AGIS) as discussed in [43] are qualitatively very different from our scheme. As such, we can compare only the scales, but not the mechanism. They generate a phase difference $\sim 10^{16} h_+$ for the space based detector [42] with baseline size $L \sim 10^7$ m compared to our $\Delta \phi(h_{ij}) \sim 10^{17} h_+$ for a baseline size of 1 m as shown in figure 3. Again, as the mechanism of our proposal differs significantly from AGIS and related schemes the above comparison does not capture the entire effectiveness of these two proposals.

One can see from 18 that the phase output will be independent of GW frequency provided $\omega \tau_3 \sim \omega \tau_1 \ll 1$, though it will be limited by gravity gradient noise at lower frequencies (see figure 3). It is in this regime that our interferometer is most sensitive to GWs. The frequency scaling of detectability is understood by noting it is susceptible to the wave’s time-averaged amplitude, which tends to zero for higher frequencies. As such, higher frequency GWs can be detected by using shorter time detectors, as seen in figure 3, albeit with a lower sensitivity without also increasing the magnetic field gradient and mass. Note that we define a detectable strain by $\Delta \phi(h_{ij}) \geq 1/\sqrt{N}$ for N particles traversing the interferometer in series (and/or several interferometers in parallel). Further note that around 10 – 10^4 Hz, LIGO is already

performing [67], while there are undetected lower frequency GW sources [68]. Our interferometer will be complementary in part of the range of LISA [38] (10^{-6} –10 Hz) for an underground implementation or all of its range for a space based interferometer.

8. Practical implementation

While the sensor we have proposed is ambitious in its scope, there does not appear to be any fundamental or insurmountable obstacle to its creation using current and near future technologies. Furthermore, we are primarily looking to show its ‘in principle’ feasibility by presenting an example scheme for realising the interferometer. For the remainder of this article we will outline the techniques which can be employed to create such an interferometer. We will discuss the primary sources of decoherence which act to destroy the superposition as well as consider the primary sources of noises in the phase output signal. This will be used to put limits on the tolerable noise and fluctuations of the experimental parameters such as mass fluctuations from one particle to the next and timings. On top of the constraints and methods discussed below, the creation of this interferometer will require further work to ensure excellent surface termination to reduce dangling bonds, motional decoupling and a method for the creation of a beam of flying diamond among further experimental advances on which work is ongoing [69] in the relatively new field of large mass interferometry.

To realise the proposed interferometer a magnetic field gradient ($\partial_x \mathbf{B}$) is used to create the spatial superposition of size $\Delta x = a\tau_1^2$ with $a = g_{NV}\mu_B\partial_x \mathbf{B}/m$ where g_{NV} is the Landé g factor and μ_B is the Bohr magneton [18]. For large mass interferometry to carry advantage over atoms, Δx must be kept ~ 1 m even while m increases. To this end, if we are to keep $\tau_1 \approx 0.73$ s as is required to achieve our maximum GW sensitivity (see figure 3) a magnetic field gradient, $\partial_x \mathbf{B}$ of 10^6 Tm $^{-1}$ is needed. Such a large magnetic field gradient could be created using a current carrying wire. We however propose the use of dual overhead wires. This allows for a more uniform magnetic field gradient to be maintained while increasing the distance between the interferometric particles and the wires, so reducing spurious forces. These wires would have to be arranged in many small horizontal sections such that they approximately follow the path of the non-zero spin interferometer arm, as shown in figure 1. This allows it to always remain proximal to the non-zero spin interferometer arm, generating a sufficiently large magnetic field gradient without also requiring an unreasonably large magnetic field. This requires a large current, which will necessitate the use of carbon nanotube-metal composites, which can support a current density of up to $\rho_I = 10^{13}$ Am $^{-2}$ [70]. The magnetic field gradient amplitude from a single wire is

$$B = \frac{\mu_0 I}{2\pi D}$$

$$\partial_x B = \frac{\mu_0 I}{2\pi D^2} = \frac{\mu_0 \rho_I \tilde{r}^2}{2(\tilde{r} + \Lambda)^2} \approx \frac{\mu_0 \rho_I}{8} \sim 10^6 \text{ Tm}^{-1} \quad (19)$$

where here D is the distance between the centre of the wire and the point at which the magnetic field strength is measured, \tilde{r} is the radius of the wire, Λ is the distance from the surface of the wire and we have taken ($\Lambda = \tilde{r}$). In this way, the primary concern to creating the large magnetic field gradients necessary are the current stability and the distance Λ required to eliminate other interactions, such as the patch potential and Casimir interactions, importantly this distance simply sets the thickness required, and does not limit the theoretical possibility of achieving the required magnetic field gradient. To generate a sufficiently uniform magnetic field gradient we propose many small pairs of overhead wires are used which modifies the experienced magnetic field gradient slightly. However, for clarity and as this is a simple proof of concept argument being presented, a simpler (single bent wire) set-up will be discussed in detail below as numbers wise, the gradient strength, noise and decoherence are effectively the same.

8.1. Decoherence

The primary sources of decoherence for the spatial superposition states will be scattering of air molecules and black-body emission giving ‘which path’ information. The spatial coherence can offer a huge window using low pressure $\sim 10^{-14}$ Pa (with lower achieved previously in cryogenically cooled systems [71]) and low internal temperature ~ 50 mK. This is achievable, for example, in a dilution fridge [72] or using laser cooling [62, 63]. For a mass of $\sim 10^{-17}$ kg and 100 nm radius, using the results of [73], scattering rates are calculated to be 0.006 Hz due to scattering of air molecules and 0.06 Hz due to black-body photon emission. The electron spin coherence at 10 mK can also reach 1 s with dynamical decoupling [74, 75] (partially present here due to spin flipping pulses, and further extendable by applying pulses to the spin bath [76].

The scale of the superpositions considered here are consistent with stochastic GW induced decoherence as we use mesoscopic objects [77].

The proposed set-up brings together state of the art magnetic field gradient, pressure and internal temperature, all having been realized individually. Sending nanodiamonds through low pressure is still being developed, as well as combining free flight with cryogenics [72].

8.2. Gravitational signals as noise

By construction, our interferometric signal only depends on the relative phase between the two arms and thereby is immune to thermal and seismic noise in $|\psi(0)\rangle$. Thus for the most sensitive proposed interferometer (for GWs), the phases due to frame dragging and Newtonian potential type sources (including gravity gradients [78]) are the primary noise. There can also be further noise sources due to the implementation, for example particle–particle and particle–magnet Casimir, patch potential and gravitational interactions.

In the following, we will consider the most challenging to detect signals (GWs) for which the highest strain sensitivity of $h_+ \sim 10^{-17}$ occurs for *single* masses of $\sim 10^{-17}$ kg, each traversing the interferometer one at a time. We can stretch this to $h_+ \sim 10^{-18}$ by considering $N = 400$ masses traversing the interferometer in series over the duration of the interferometer (τ_3), one after another. This can be achieved by successively cooling [59–63] and injecting one particle every ~ 10 ms. This then sets the signal strength which all noises must be kept below (we will discuss below how this can be met). Further, for low frequency GW detection, say for GWs of frequency ~ 10 mHz one can do ~ 100 repeats of this interference during the period of the gravitational wave. This will improve the sensitivity by an order of magnitude so as to bring the detector into the range of detection of massive binaries at the above frequency [79]. One can further improve sensitivity by another factor of $1/\sqrt{N}$ by using N interferometers in parallel. This also corresponds to the most ambitious setting for the sensor, with a mass $m = 10^{-17}$ kg, time $\tau_1 = 0.73$ s, $v_x = a\tau_1 = 1.35\text{ms}^{-1}$.

Firstly, a simple source of noise in any signal, GW signals included, is due to parameter fluctuations from one run to the next. With this in mind it is only necessary to consider the largest phase effect (the Newtonian potential) as it will magnify any uncertainty the most. It should be noted that, although not immediately obvious from 5 or 8, the first order Newtonian phase is independent of the particles mass, this is due to the inverse scaling of the superposition size with the mass. Furthermore these noises can be suppressed by orientating the interferometer to be perpendicular to the Newtonian potential gradient (parallel with the ground). This gives a phase uncertainty $\delta\phi$ due to mass (δm), distance (δR), superposition size ($\delta(\Delta x)$) and timing ($\delta\tau_1$) uncertainty of approximately

$$\delta\phi \approx \frac{23\delta m M G \sin(\alpha)}{15\hbar R^3} \Delta x^2 \tau_1 + \frac{2m M G \sin(\alpha)}{\hbar R^2} \left(\frac{-2\delta R}{R} \Delta x \tau_1 + \delta(\Delta x) \tau_1 + \Delta x \delta\tau_1 \right) \quad (20)$$

where $\alpha = 0$ when the interferometer is exactly perpendicular to the local Newtonian potential gradient. This was derived from equation (8) allowing for variations in the experimental parameters and orientating the interferometer relative to the local Newtonian gravitational potential. Given that an orientation uncertainty ≤ 1 pRad is measurable [80], thus $|\sin(\alpha)| \leq 10^{-12}$ is achievable, the mass, distance, separation and timing fluctuation would have to be kept below $\delta m \leq 10^{-18}$ kg, $\delta R \leq 0.1$ m, $\delta(\Delta x) \leq 10$ nm and $\delta\tau_1 \leq 1$ ns respectively to ensure $\delta\phi$ is kept below the detectable limit, that is, to ensure $\delta\phi \leq 0.1$. Variations in otherwise known (systematic) phases can be countered through a careful characterisation of system parameters and/or modifications of the interferometric setup.

We can note that some noises can be identified due to the unique functional dependences (specifically how they scale with a , v_y and τ_1) of the 5 identified signals (5–7) the individual types of signals could be identified separately by a network of interferometers allowing them the signal to be filtered out from them. Of specific note is that by setting $v_y = 0$, 6 becomes zero. Doing so however will limit the ability to introduce more than one particle into the interferometer at a time, making the sensitivity (and noise ceiling) $\Delta\phi = 1$ for a single run of a single interferometer. Furthermore, certain external noises can be actively cancelled. First order signals can be detected and cancelled by a symmetric detector (using an initial spin superposition $\frac{1}{\sqrt{2}} [|+1\rangle + |-1\rangle]$) insensitive to second order effects and GWs. Here by first order signals we are referring to terms in 5 and 6 which are a function of a single derivative. This can be done as these are the only terms which a symmetric interferometer is sensitive to (the $\propto a^2$ terms cancel when the difference is calculated), as such, these noises can be treated as signals which can be subtracted from the total phase output. The second order Newtonian potential term can also be approximated by the use of slightly displaced symmetric interferometers. These would again be insensitive to GWs and would result in third order effects being left in the noise. This method of active cancellation is also only an approximation. For example consider a source located a distance R from the primary detector, with secondary, symmetric

interferometers located at $R \pm s$ from the source. The signal at the central asymmetric interferometer would be approximately the average of signal at each symmetric interferometer either side of it. This approximate signal can be used to cancel the phase noise, thus reducing it by a factor $\epsilon^{(1)}$ which encompasses how close the approximation is. To determine $\epsilon^{(1)}$ we can expand the signal in orders of $\frac{s}{R}$ from the central, asymmetric interferometer giving

$$\begin{aligned}\epsilon^{(1)} &= \frac{\delta\phi^{(1)}(R) - \frac{1}{2}(\delta\phi^{(1)}(R+s) + \delta\phi^{(1)}(R-s))}{\delta\phi^{(1)}(R)} \\ &= 1 - \frac{1}{2} \left(\left(1 + \frac{s}{R}\right)^{1/2} + \left(1 - \frac{s}{R}\right)^{1/2} \right) \\ &\approx 1 - \frac{1}{2} \left(1 + \frac{s}{2R} - \frac{s^2}{8R^2} + 1 - \frac{s}{2R} - \frac{s^2}{8R^2} \right) \\ &= -\frac{s^2}{8R^2}.\end{aligned}\tag{21}$$

Take for example the movement of a 1 kg mass, a distance of 1 m away from the sensor and aligned with the interferometers x axis (the direction it is sensitive in). If we consider the primary interferometer as having a symmetric interferometer above and below it at a distance of $s = 1$ cm then by 11 its movement would have to be less than $d = 10^{-10}$ m without any active cancelation, however, with cancelation this becomes $d = 10^{-5}$ m, a still significant, but far less difficult value.

8.3. Gravity gradient noise

Distant Newtonian potential fluctuations are known as Gravity gradient noise (GGN) [81, 82]. This is known to be one of the primary noise sources which limit GW detections in present day GW antennas, particularly at the low frequencies. Gravity gradient noise is due to seismic waves causing variations in the local gravitational field. These seismic waves are not as dramatic as earthquakes, but stochastic fluctuations in the local density and surface fluctuations in the surrounding ground. It is difficult to say anything too specific about gravity gradient amplitudes as these are known to be highly location dependent [83]. We will be following closely the analysis performed in [84, 85], combined with measured gravity gradient accelerations [86, 87] as well as consider how well we could hope to cancel such effects.

Consider the effect of a fluctuation in the atmospheric or ground density $\Delta\rho$ of some volume V , where for the example of ground based fluctuations of wavelength λ and height ξ , $V = \lambda^2\xi$, at some distance r from our interferometer. This will yield an anomalous acceleration of magnitude

$$a = \frac{G\Delta\rho V}{r^2} \cos(\beta) \sin(\gamma)\tag{22}$$

where β and γ are the polar coordinates of the disturbance with the coordinate origin located at the detector. This was derived by considering the standard formula for acceleration due to the Newtonian gravitational interaction and that the interferometer is sensitive in only a single direction. Thus the trigonometric dependences are due to the directional sensitivity of the detector. To simplify the analysis we will consider all regions of fluctuation as independent and so consider the joint effect by adding the squared acceleration. We will also consider a minimum distance, r_0 , that is our interferometer to be within a cavity in which there are no density fluctuations. Considering initially an interferometer located at the surface of the Earth, then the square of the expected acceleration will be

$$a^2 \approx G^2 \Delta\rho^2 V^2 \int_0^{\frac{\pi}{2}} \int_{-\pi}^{\pi} \int_{r_0}^{\infty} \frac{1}{r^4} \cos^2(\beta) \sin^2(\gamma) r^2 \sin(\gamma) dr d\beta d\gamma\tag{23}$$

$$\rightarrow a \approx \sqrt{\frac{2\pi}{3}} \frac{G\Delta\rho V}{\sqrt{r_0}}.\tag{24}$$

Now if the interferometer is placed underground at a depth d this becomes

$$a^2 \approx G^2 \Delta\rho^2 V^2 \int_0^{\frac{\pi}{2}} \int_{-\pi}^{\pi} \int_{d/\cos(\gamma)}^{\infty} \frac{1}{r^2} \cos^2(\beta) \sin^3(\gamma) dr d\beta d\gamma\tag{25}$$

$$\rightarrow a_{\text{u}} \approx 0.6 \frac{a\sqrt{r_0}}{\sqrt{d}}.\tag{26}$$

and so we can estimate the phase noise in our underground sensor. Using the measured median results in [86, 87] of $a_{\text{surface}} = 3 \times 10^{-11} \text{ms}^{-2}$ for fluctuations occurring at 1 mHz we can estimate the underground phase noise due to a stochastically varying local acceleration assuming $r_0 = 1 \text{ m}$ and $d = 100 \text{ m}$ as

$$\delta\phi^{(1)} \sim \frac{2m}{\hbar} \left(0.6 \frac{a\sqrt{r_0}}{\sqrt{d}} \right) \Delta x \tau_1 \quad (27)$$

$$\sim 2 \times 10^5 \quad (28)$$

which is clearly quite significant. It is also worth noting that ‘quiet’ (low GGN noise) sites can have noise values two orders of magnitude smaller [84]. There will also be second order effects ($\delta\phi^{(2)}$) where the local gravity varies across the interferometer which will be approximately a factor of $\frac{\Delta x}{\lambda} \sim 0.001$ smaller for typical fluctuation wavelengths $\lambda = 1 \text{ km}$ [83] giving $\delta\phi^{(2)} \sim 2 \times 10^2$ at 1 mHz.

These can however be measured and cancelled using symmetric implementations of the interferometer as discussed above, hence the phase noise will then be $\delta\phi^{(1)} \rightarrow \epsilon^{(1)} 10^5 \sim 10^{-4}$ for $s = 0.01 \text{ m}$ which is sufficient to allow detections in this frequency spectrum. There is still the issue of the second order phase variations ($\delta\phi^{(2)}$). These can similarly be approximated, this time by two symmetric interferometers, now spread in the ‘x’ direction, and taking the difference between them divided by the distance between them. As the two interferometers would have to be spread further apart to make room for the original interferometer then before they will only accurately measure linear change in g across the interferometer. This suggest the error in the phase due to GGN after both methods of cancellations are used will be effectively the third order GGN effect, which will be a further $\frac{\Delta x}{\lambda}$ smaller than the second order effect, giving $\delta\phi^{(3)} \sim 10^{-1}$ at 1 mHz frequency. This is still significant and as such gravity gradient noise will create an effective noise floor to the sensitivity of our detector. To determine how it effects our sensitivity at other frequencies we use the scaling provided in [84] of $1/\sqrt{f}$ to generate the noise floor after cancelling $\delta\phi^{(1)}$ and $\delta\phi^{(2)}$ as discussed above, for all relevant frequencies. The resulting GGN signal is then

$$\delta\phi^{(3)} \sim \left(\frac{\Delta x}{\lambda} \right)^2 \frac{2m}{\hbar} \left(0.6 \frac{\sqrt{r_0}}{\sqrt{d}} \times \frac{3 \times 10^{-11}}{\sqrt{f/1 \text{ mHz}}} \right) \Delta x \tau_1 \quad (29)$$

$$\approx \frac{8 \times 10^{-3}}{\sqrt{f/1 \text{ Hz}}} \quad (30)$$

for the $m = 10^{-17} \text{ kg}$ interferometer used in figure 3, this also shows that the optimal sensitivity here is in the 0.04–3 Hz range. Note this also matches closely with the median GGN spectra given in [86].

This is a somewhat crude model, treating both ground and atmospheric fluctuations at once, assuming uncorrelated fluctuations and integrating over each cell rather than summing. However as we are using actual measured results for a_{surface} and in effect only concerned with the scaling with r and d , we are unlikely to be lead astray by our model. Also we are using the measured median GGN spectra and as such likely over estimating the noise as it would actually effect our interferometer as we would intend for it to be placed at a ‘quiet’ site with low GGN. Furthermore we can note that such a method of measuring and cancelling noise can be applied to other GW sensors, potentially extending the ground based observable frequencies in all GW sensors.

8.4. Heisenberg uncertainty noise

Another key noise source in standard GW detectors is the fundamental noise due to the Heisenberg uncertainty limit. For simplicity we will consider the mass to be in a coherent state saturating the uncertainty principle, that is,

$$\sigma_x \sigma_p = \frac{\hbar}{2} \quad (31)$$

$$\sigma_p = \sqrt{\frac{m\omega\hbar}{2}} \approx 7 \times 10^{-24} \text{ kg ms}^{-1} \quad (32)$$

$$\sigma_x = \sqrt{\frac{\hbar}{2m\omega}} \approx 7 \times 10^{-12} \text{ m}. \quad (33)$$

where the particle is assumed to be released from a 100 kHz trap. Beginning with position uncertainty there are two potential manners in which this could impact the final result, the first is uncertainty in the initial position giving

$$\delta(\Delta\phi(h_{00})) \approx \left(\frac{2mMG}{\hbar} a\tau_1^3\right) \left(\frac{1}{(R)^2} - \frac{1}{(R + \sigma_x)^2}\right) \sin(\alpha) \quad (34)$$

$$\approx \left(\frac{4mMG\sigma_x}{\hbar R^4} a\tau_1^3\right) \sin(\alpha) \sim 10^{-7} \sin(\alpha) \quad (35)$$

where again α is the angle between the interferometer's x axis and the local plane of constant Newtonian potential. The second manner in which position uncertainty due to HUP could manifest as noise is by impacting the overlap between the particle. However it is known [18] that this cannot effect the result as the phase difference is independent of the initial spacial state.

Along similar lines we can consider how the initial momentum HUP uncertainty results in phase uncertainty. This gives

$$\delta(\Delta\phi_{h_{00}}) \approx \frac{8MG\sigma_p a\tau_1^4}{\hbar R^3} \sin(\alpha) \sim 10^5 \sin(\alpha) \quad (36)$$

as such provided $\alpha \ll 10^{-5}$ this is also not an issue. As it is anticipated $\alpha \sim 10^{-12}$ [80] the HUP is not anticipated to be a limiting factor.

8.5. Particle–particle interactions

Any electrostatic interactions can be eliminated as the particle charge can be measured and modified down to the single electron level [58]. The more concerning interactions will be particle–particle and particle–magnet interactions. The particle–particle interactions are kept in check by ensuring the particle flux is low where here the flux is defined as the number of particles through the interferometer per second. The phase uncertainty it introduces is primarily due to the inter-particle Casimir interaction. It however can be minimised by ensuring a large enough v_y , for example, considering the effective Casimir potential (U_C) between two diamond ($\epsilon = 5.7$) spheres of radius \bar{R} a distance d apart as

$$U_C = \frac{23\hbar c \bar{R}^6}{4\pi d} \left(\frac{\epsilon - 1}{\epsilon + 2}\right)^2 \quad (37)$$

then provided $v_y = 10 \text{ ms}^{-1}$ then a flux $N = 1000$ will lead to a phase uncertainty of approximately 0.002 rad with a phase sensitivity to the 0.03 radian level. When $v_y = 1 \text{ ms}^{-1}$ the highest allowable flux is about $N = 90$ which gives a phase uncertainty of approximately 0.05 rad with sensitivity of approximately 0.1 rad. To this end we have considered $N = 400$ with $v_y = 10 \text{ ms}^{-1}$ as sufficient to ensure the particle–particle interactions are negligible while also gaining phase sensitivity, with larger fluxes yielding phase sensitivity which would likely lost to other noises discussed above. Note that such large values for v_y can be achieved for a polarizable particle (e.g. nanodiamond) using rapid acceleration in a pulsed optical field [88].

8.6. Magnetic field fluctuations

Fluctuations of the magnetic field and its gradient will effect the interferometer in a number of differing ways: modify Δx , stop the interferometer closing perfectly and through the phase fluctuation associated with variations in the magnetic potential energy.

The source of the magnetic field fluctuations will be due to variations in the current through the wire taking $I \rightarrow I + \delta I$. Such fluctuations will translate to variations in the applied acceleration δa given by

$$\frac{\delta a}{a} = \frac{\delta I}{I}. \quad (38)$$

Now if such fluctuations occur at time spans similar to the total interferometry time ($\tau_3 = 4\tau_1$) than they will automatically be cancelled to the alternating direction of the acceleration. Similarly if they occur much faster than again they will on average cancel throughout the interferometry process. As such the most significant position fluctuations occur if the sign of δI changes at times $t = \tau_1$ and then again at $t = \tau_2$ suggesting a characteristic time span of $2\tau_1$ such that its contribution to the acceleration never cancels. In this instance we have

$$\frac{\delta(\Delta x)}{\Delta x} = \frac{\delta a}{a} = \frac{\delta I}{I} \quad (39)$$

although, if multiple particles are traversing the interferometer in series then for a later particle this effect would smaller or cancel completely, a detail we will neglect here so that we are not underestimating the noise. In the context of the Newtonian potential variations from one run to the next we found that we require $\delta(\Delta x) \leq 10$ nm (cf section 8.2), which, given the maximum superposition size is $\Delta x = 1$ m, sets a limit to the current variation $\delta I = 10^{-8}I$ over a time-scale of $2\tau_1 \approx 1.5$ s. Now the ensure this is not exceeded the experimentalists would simply have to monitor the current with an ammeter to ensure drift is kept below this level.

Furthermore we can consider the current fluctuation due to thermal effects within the conducting wire by considering Johnson–Niquist noise which gives the current noise through the wire as

$$\delta I = \sqrt{\frac{4k_B T \Delta f}{R}} \quad (40)$$

where k_B is Boltzmann's constant, T the temperature of the wire, $\Delta f \sim 1$ Hz the bandwidth for noise and $R \sim 22$ k Ω is the resistance of the wire [89]. This gives a current noise of $\delta I \sim 10^{-12}$ A if the wire is maintained at room temperature. This is likely to be well below the required noise floor, even with the wire heating up well above room temperature.

This will also then lead to the particles overlapping only up to the bound given approximately by $\delta(\Delta x)$. However using the results derived below we can conclude $\delta(\Delta x) \sim 10^{-15}$ m, far below the assumed wavepacket spread due to Heisenberg uncertainty of $\sigma_x \sim 10^{-11}$ m and so is not of significant concern.

Finally we can consider the phase fluctuation due to the magnetic field coupling. This phase due to the coupling between an electronic spin and an aligned magnetic field is given by

$$\phi_{\vec{B}} = \frac{\vec{\mu} \cdot \vec{B}t}{\hbar} = -\frac{egS}{2m_e\hbar} \frac{\mu_0 I}{2\pi D} t \quad (41)$$

where e and m_e are the charge and mass of an electron, $g \approx 2$ is the gyromagnetic ratio and S is the spin angular momentum. Now as the spin state is reversed throughout the interferometer, the total phase will effectively unwind itself, up to the stability in both the mean magnetic field strength and timing accuracy. In this way the phase difference will be $\Delta\phi_{\vec{B}} = 0$ up to some stochastic fluctuations given by

$$\begin{aligned} \delta(\Delta\phi_{\vec{B}}) &= \frac{eg\hbar}{2m_e\hbar} \times \frac{\mu_0\delta I}{2\pi D} \tau_3 + \frac{eg\hbar}{2m_e\hbar} \times \frac{\mu_0\rho_I\pi D^2}{2\pi D} \delta t \\ &\sim \frac{10^{-7} \text{ m}}{D} + 10^{17} \text{ m}^{-1} \text{ s}^{-1} D\delta t. \end{aligned} \quad (42)$$

Now the first term implies a restriction on the distance between the centre of the wire and the particle of $D \geq 1$ μm while the second term implies a limit on the timing uncertainty of $\delta t \ll 10^{17}D \text{ m}^{-1} \text{ s}$. So, taking $D = 2 \times 10^{-5}$ m, thus requiring a current of $I \approx 2000$ A and magnetic field magnitude of $B = 40$ T, a timing uncertainty of $\delta t \leq 10^{-13}$ s is required. This is certainly a difficult requirement, but does not seem completely unreasonable given the historical achievement of pico-second (10^{-12} s) timings with microwave lasers [90] with femto-second also achieved more recently [91].

Each small section of current carrying wire pair will have to be controlled independently and thus will have an independent current fluctuating stochastically about the intended value I . Therefore, there is no independent noise at frequencies lower than that which corresponds to the time each wire pair controls the particle-noise at such frequencies essentially corresponds to the sum of noises from blocks of consecutive wires. Thus we do not need to consider them separately; considering the noise at the frequency corresponding to the time each wire pair controls the particle suffices. In this case, the wire pair controls the motion of the particle for typically $t_{\text{wire}} = 7$ μs to ensure the particle sees a uniform, linear magnetic field gradient throughout the interferometry process. This corresponds to a noise frequency of $f_{\text{wire}} \sim 1.4 \times 10^5$ Hz. Over the total time of the experiment ~ 1 s, the uncertain part of the Zeeman phase accumulated will be a summative random walk type phase. Here each wire interval is responsible for a step in the random walk. For this to be negligible, we require the random part of the magnetic field magnitude at the frequency f_{wire} to be $\delta B(f_{\text{wire}}) < \frac{\hbar}{\mu_B} \sqrt{f_{\text{wire}}} \sim 4$ nT (alternatively, simply keeping track of the magnetic field fluctuations to this accuracy will suffice). This corresponds to a current uncertainty of $\delta I(f_{\text{wire}}) < 20$ μA at the frequency of f_{wire} . For frequencies $f > f_{\text{wire}}$, the constraint on $\delta B(f) \leq 4\sqrt{f/f_{\text{wire}}}$ nT will only be easier to satisfy. Additionally, the fluctuation in the gradient will also cause an uncertainty in the particle's

position of

$$\delta(\Delta x) = \frac{\delta I t_{\text{wire}}^2 \Delta x}{I \tau_1^2} \approx \frac{\delta I \times 10^{-10}}{I} \quad (43)$$

which, by requiring $\delta(\Delta x) \ll \sigma_x$, bounds the high frequency (MHz) magnetic field fluctuations δI to $\delta I \ll 20$ A. This can be extrapolated to give a general bound, frequency dependent bound of

$$\delta I(f) \leq \frac{2 \times 10^3 \text{ A Hz}^{-1/2}}{\sqrt{f}}. \quad (44)$$

8.7. Particle–magnet Casimir interaction

To model the particle–magnet Casimir induced phase fluctuations we can note that, as the particle radius is $\bar{R} \sim 10^{-7}$ m and the particle–magnet surface distance is kept at $\Lambda = 10^{-5}$ m, the particle–magnet system can be considered to be in the long range limit, the path phase difference of [92]

$$\Delta \phi_{\text{Casimir}} = \frac{23c\bar{R}^3}{4\pi\Lambda^4} \tau_3 \sim 10^6 \text{ rad} \quad (45)$$

where c is the speed of light and τ_3 is the total interferometry time as shown in figure 1. While this is significant, it is a constant phase provided the separation distance is also kept constant it can be normalised for in the output. This however requires certainty in the particle–magnet separation to be $\sim 10^{-11}$ m while the aforementioned timing stability is sufficient here. This also leads to a maximum path displacement of $\sim 10^{-3}$ m over the length of the interferometer leading to the two state not overlapping without also adjusting the spin-0 arm of the interferometer. This displacement will be stable to the same level as the phase however and so should not limit the ability to completely overlap the two.

Patch potentials refer to electrostatic interactions between regions of non-zero charge on a globally charge neutral object. The patch potential interactions can largely be dealt with by using single crystal particles as the interferometry masses. The particle–magnet patch potential interaction will be further minimised by the geometry of the system. The patch potential force [93] scales as

$$F \propto \frac{\bar{R}e^{\Lambda/a}}{\sinh(\Lambda/a)} \quad (46)$$

where again $\bar{R} \sim 10^{-7}$ m is the particle radius, $\Lambda \sim 10^{-4}$ m is the particle–magnet separation and here $a < \bar{R}$ is the size of the patch potential. This exponential suppression means that the patch potential is effectively negligible. Furthermore since the particle can move along the magnet, and by initialising the particles as physically spinning any patch potential interactions can be further averaged out. Finally if the particle is constructed out of a single crystal these patch potential effects would be negligible.

9. Conclusion

We have presented the possibility of using the interferometry of mesoscopic objects (say, objects of mass $\sim 10^{-17}$ kg) to detect both first and second order derivatives of the space-time metric in a compact setup. We have found that for mesoscopic masses, such interferometry is not only sensitive to the Newtonian potential, Earth’s frame dragging, but also extremely weak signals such as mid frequency GWs for a ground based detector, and low frequency GWs for a space based detector. We have presented an example form for such a mesoscopic mass interferometer and presented the expected sensitivity for our device. In designing our example detector, we have identified the requirements which must be met to mitigate the known sources of noise, such as GGN, uncertainty principle, Casimir and patch-potential interactions. The SG principle of the specific interferometer design implies that simply by changing the orientation of a magnet, the whole interferometer is re-oriented to both identify the angular origin of sources and couple to different components of the metric tensor. Furthermore, the manner in which the phase difference accumulated due to the Newtonian potential and GW signals scale with the experimental parameters a and τ_1 points to an important and fundamental difference between this type of interferometer and light based interferometers. This difference provides an avenue to further improve GW sensitivity while reducing many noise sources, including GGN. The compactness means that whole GW sensitive interferometers can be put in a single vibrational isolation platform [67] and large networks of interferometers can be built to identify and cancel noise. Less demanding values for $\partial_x \vec{B}$ and the coherence times suffice to detect the less demanding components such as h_{00} or for accelerometry (e.g. $\partial_x \vec{B} = 10^4 \text{ T m}^{-1}$, $\tau_1 \sim 70$ ms, 10^{-18} kgs and $\Delta x = 1$ mm can already detect both the Newtonian curvature and the Earth’s frame dragging). Attempts to build

the most ambitious limit of the interferometers, namely, for GW detection with superpositions of 10^{-17} kg masses as discussed here will also push the limits of macroscopicity of superpositions as defined in [94] to $\mu \approx 26$ (where atomic and macromolecular interferometry have achieved $\mu \approx 11$ [95] and $\mu \approx 14.5$ [96] respectively, with an actual Schrodinger cat experiment corresponding to $\mu \approx 57$). This will constrain intrinsic collapse models [20, 95] to an electron coherence time $\tau_e \sim \times 10^{26}$ s at a critical length scale $\hbar/\sigma_q \sim 1$ m. We may be able to test short distance modifications of gravity [97, 98], and the gravitational self-localization of wavefunctions [99, 100].

Acknowledgments

AM's research is funded by the Netherlands Organisation for Scientific Research (NWO) Grant number 680-91-119, GWM is supported by the Royal Society. We acknowledge EPSRC Grant No. EP/M013243/1. PFB and SB would like to acknowledge EPSRC Grants No. EP/N031105/1 and EP/S000267/1. RJM is supported by a UCL departmental studentship. We would also like to thank Ron Folman for his insightful discussions regarding the experimental implementation of large magnetic field gradients using current carrying wires.

ORCID iDs

Ryan J Marshman  <https://orcid.org/0000-0001-8860-1510>

Anupam Mazumdar  <https://orcid.org/0000-0002-0967-8964>

References

- [1] Cronin A D, Schmiedmayer J and Pritchard D E 2009 Optics and interferometry with atoms and molecules *Rev. Mod. Phys.* **81** 1051–129
- [2] Gerlich S *et al* 2007 A Kapitza–Dirac–Talbot–Lau interferometer for highly polarizable molecules *Nat. Phys.* **3** 711
- [3] Bose S, Jacobs K and Knight P L 1999 Scheme to probe the decoherence of a macroscopic object *Phys. Rev. A* **59** 3204
- [4] Armour A D, Blencowe M P and Schwab K C 2002 Entanglement and decoherence of a micromechanical resonator via coupling to a Cooper-pair box *Phys. Rev. Lett.* **88** 148301
- [5] Marshall W, Simon C, Penrose R and Bouwmeester D 2003 Towards quantum superpositions of a mirror *Phys. Rev. Lett.* **91** 130401
- [6] Sekatski P, Aspelmeyer M and Sangouard N 2014 Macroscopic optomechanics from displaced single-photon entanglement *Phys. Rev. Lett.* **112** 080502
- [7] Romero-Isart O, Mathieu L J, Quidant R and Cirac J I 2010 Toward quantum superposition of living organisms *New J. Phys.* **12** 033015
- [8] Romero-Isart O, Pflanzner A C, Blaser F, Kaltenbaek R, Kiesel N, Aspelmeyer M and Cirac J I 2011 Large quantum superpositions and interference of massive nanometer-sized objects *Phys. Rev. Lett.* **107** 020405
- [9] Khalili F, Danilishin S, Miao H, Müller-Ebhardt H, Yang H and Chen Y 2010 Preparing a mechanical oscillator in non-gaussian quantum states *Phys. Rev. Lett.* **105** 070403
- [10] Scala M, Kim M S, Morley G W, Barker P F and Bose S 2013 Matter-wave interferometry of a levitated thermal nano-oscillator induced and probed by a spin *Phys. Rev. Lett.* **111** 180403
- [11] Bateman J, Nimmrichter S, Hornberger K and Ulbricht H 2014 Near-field interferometry of a free-falling nanoparticle from a point-like source *Nat. Commun.* **5** 4788
- [12] Yin Z Q, Li T, Zhang X and Duan L M 2013 Large quantum superpositions of a levitated nanodiamond through spin-optomechanical coupling *Phys. Rev. A* **88** 033614
- [13] Pino H, Prat-Camps J, Sinha K, Venkatesh B P and Romero-Isart O 2018 On-chip quantum interference of a superconducting microsphere *Quantum Sci. Technol.* **3** 025001
- [14] Clarke J and Vanner M R 2019 Growing macroscopic superposition states via cavity quantum optomechanics *Quantum Sci. Technol.* **4** 014003
- [15] Ringbauer M, Weinhold T J, White A G and Vanner M R 2016 Generation of mechanical interference fringes by multi-photon quantum measurement (arXiv:1602.05955)
- [16] Khosla K E, Vanner M R, Ares N and Laird E A 2018 Displacement electromechanics: how to detect quantum interference in a nanomechanical resonator *Phys. Rev. X* **8** 021052
- [17] Kaltenbaek R, Hechenblaikner G, Kiesel N, Romero-Isart O, Schwab K C, Ulrich J and Aspelmeyer M 2012 Macroscopic quantum resonators (MAQRO) *Exp. Astron.* **34** 123–64
- [18] Wan C, Scala M, Morley G W, Rahman A T M A, Ulbricht H, Bateman J, Barker P F, Bose S and Kim M S 2016 Free nano-object Ramsey interferometry for large quantum superpositions *Phys. Rev. Lett.* **117** 143003
- [19] Romero-Isart O 2017 Coherent inflation for large quantum superpositions of levitated microspheres *New J. Phys.* **19** 123029
- [20] Roger P 1996 On gravity's role in quantum state reduction *Gen. Relativ. Gravit.* **28** 581–600
- [21] Bassi A, Lochan K, Satin S, Singh T P and Ulbricht H 2013 Models of wave-function collapse, underlying theories, and experimental tests *Rev. Mod. Phys.* **85** 471
- [22] Bose S *et al* 2017 Spin entanglement witness for quantum gravity *Phys. Rev. Lett.* **119** 240401
- [23] Marletto C and Vedral V 2017 Gravitationally induced entanglement between two massive particles is sufficient evidence of quantum effects in gravity *Phys. Rev. Lett.* **119** 240402
- [24] Colella R, Overhauser A W and Werner S A 1975 Observation of gravitationally induced quantum interference *Phys. Rev. Lett.* **34** 1472

- [25] Anandan J 1984 Effect of newtonian gravitational potential on a superfluid josephson interferometer *Phys. Rev. B* **30** 3717
- [26] McGuirk J M, Foster G T, Fixler J B, Snadden M J and Kasevich M A 2002 Sensitive absolute-gravity gradiometry using atom interferometry *Phys. Rev. A* **65** 033608
- [27] Qvarfort S, Serafini A, Barker P F and Bose S 2018 Gravimetry through non-linear optomechanics *Nat. Commun.* **9** 3690
- [28] Armata F, Latmiral L, K Plato A D and Kim M S 2017 Quantum limits to gravity estimation with optomechanics *Phys. Rev. A* **96** 043824
- [29] Peter A, Overstreet C, Kovachy T, Brown D D, Hogan J M and Kasevich M A 2017 Phase shift in an atom interferometer due to spacetime curvature across its wave function *Phys. Rev. Lett.* **118** 183602
- [30] Werner S A, Staudenmann J L and Colella R 1979 Effect of Earth's rotation on the quantum mechanical phase of the neutron *Phys. Rev. Lett.* **42** 1103–06
- [31] Anandan J 1977 Gravitational and rotational effects in quantum interference *Phys. Rev. D* **15** 1448
- [32] Dimopoulos S, Graham P W, Hogan J M and Kasevich M A 2008 General relativistic effects in atom interferometry *Phys. Rev. D* **78** 042003
- [33] Everitt C W F *et al* 2011 Gravity Probe B: Final results of a space experiment to test general relativity *Phys. Rev. Lett.* **106** 221101
- [34] Albert R 2017 Circumventing Heisenberg's uncertainty principle in atom interferometry tests of the equivalence principle *Phys. Rev. Lett.* **118** 160401
- [35] Albert R 2018 Gravitational redshift in quantum-clock interferometry (arXiv:1810.06744)
- [36] Abbott B P *et al* 2016 Observation of gravitational waves from a binary black hole merger *Phys. Rev. Lett.* **116** 061102
- [37] Harry G M LIGO Scientific Collaboration *et al* 2010 Advanced LIGO: the next generation of gravitational wave detectors *Class. Quantum Grav.* **27** 084006
- [38] Amaro-Seoane P *et al* 2017 Laser interferometer space antenna (arXiv:1702.00786)
- [39] Chiao R Y and Spiliotopoulos A D 2004 Towards migo, the matter-wave interferometric gravitational-wave observatory, and the intersection of quantum mechanics with general relativity *J. Mod. Opt.* **51** 861–99
- [40] Albert R, Brill D R, Hu B L, Misner C W and Phillips W D 2006 Gravitational wave detectors based on matter wave interferometers (MIGO) are no better than laser interferometers (LIGO) *Phys. Rev. D* **73** 084018
- [41] Foffa S, Gasparini A, Papucci M and Sturani R 2006 Sensitivity of a small matter-wave interferometer to gravitational waves *Phys. Rev. D* **73** 022001
- [42] Dimopoulos S, Graham P W, Hogan J M, Kasevich M A and Rajendran S 2008 An atomic gravitational wave interferometric sensor (agis) *Phys. Rev. D* **78** 122002
- [43] Dimopoulos S, Graham P W, Hogan J M, Kasevich M A and Rajendran S 2009 Gravitational wave detection with atom interferometry *Phys. Lett. B* **678** 37–40
- [44] Canuel B *et al* 2018 Exploring gravity with the miga large scale atom interferometer *Sci. Rep.* **8** 14064
- [45] Graham P W, Hogan J M, Kasevich M A, Rajendran S and Romani R W 2017 Mid-band gravitational wave detection with precision atomic sensors (arXiv:1711.02225)
- [46] Rätzel D, Schneiter F, Bravo D, Bravo T, Howl R, Lock M P E and Fuentes I 2018 Frequency spectrum of an optical resonator in a curved spacetime *New J. Phys.* **20** 053046
- [47] Rätzel D, Howl R, Lindkvist J and Fuentes I 2018 Dynamical response of Bose–Einstein condensates to oscillating gravitational fields *New J. Phys.* **20** 073044
- [48] Arvanitaki A and Geraci A A 2013 Detecting high-frequency gravitational waves with optically levitated sensors *Phys. Rev. Lett.* **110** 071105
- [49] Pontin A, Mourounas L S, Geraci A A and Barker P F 2018 Levitated optomechanics with a fiber fabry–perot interferometer *New J. Phys.* **20** 023017
- [50] Ando M, Ishidoshiro K, Yamamoto K, Yagi K, Kokuyama W, Tsubono K and Takamori A 2010 Torsion-bar antenna for low-frequency gravitational-wave observations *Phys. Rev. Lett.* **105** 161101
- [51] Machluf S, Japha Y and Folman R 2013 Coherent Stern–Gerlach momentum splitting on an atom chip *Nat. Commun.* **4** 09
- [52] Margalit Y, Zhou Z, Or Dobkowski, Japha Y, Rohrlich D, Moukouri S and Folman R 2018 Realization of a complete Stern–Gerlach interferometer (arXiv:1801.02708)
- [53] Amit O *et al* 2019 T^3 Stern–Gerlach matter-wave interferometer *Phys. Rev. Lett.* **123** 083601
- [54] Hammerer K and Aspelmeyer M 2015 Optomechanics: diamonds take off *Nat. Photon.* **9** 633
- [55] Neukirch L P, Haartman E V, Rosenholm J M and Vamivakas A N 2015 Multi-dimensional single-spin nano-optomechanics with a levitated nanodiamond *Nat. Photon.* **9** 653
- [56] Siyushev P *et al* 2014 Coherent properties of single rare-earth spin qubits *Nat. Commun.* **5** 3895
- [57] Liu S, Serrano D, Fossati A, Alexandre T, Ferrier A and Goldner P 2018 Controlled size reduction of rare earth doped nanoparticles for optical quantum technologies *RSC Adv.* **8** 37098–104
- [58] Frimmer M, Luszcz K, Ferreira S, Jain V, Hebestreit E and Novotny L 2017 Controlling the net charge on a nanoparticle optically levitated in vacuum *Phys. Rev. A* **95** 061801(R)
- [59] Delić U, Reisenbauer M, Dare K, Grass D, Vuletić V, Kiesel N and Aspelmeyer M 2020 Motional quantum ground state of a levitated nanoparticle from room temperature *Science* **367** 892–5
- [60] Chang D E, Regal C A, Papp S B, Wilson D J, Ye J, Painter O, Kimble H J and Zoller P 2010 Cavity opto-mechanics using an optically levitated nanosphere *Proc. Natl Acad. Sci.* **107** 1005–10
- [61] Ferialdi L, Setter A, Toroš M, Timberlake C and Ulbricht H 2019 Optimal control for feedback cooling in cavityless levitated optomechanics *New J. Phys.* **21** 073019
- [62] Rahman A T M A and Barker P F 2017 Laser refrigeration, alignment and rotation of levitated $\text{yb } 3+$: Ylf nanocrystals *Nat. Photon.* **11** 634
- [63] Mungan C E and Gosnell T R 1999 Laser cooling of solids *Advances in Atomic, Molecular, and Optical Physics* vol 40 (Amsterdam: Elsevier) pp 161–228
- [64] Henkel C, Jacob G, Stopp F, Schmidt-Kaler F, Keil M, Japha Y and Folman R 2019 Stern–Gerlach splitting of low-energy ion beams *New J. Phys.* **21** 083022
- [65] Visser M 2018 Post-newtonian particle physics in curved spacetime (arXiv:1802.00651)
- [66] Weinberg S 1972 *Gravitation and Cosmology: Principles and Applications of the General Theory of Relativity* vol 1 (New York: Wiley)

- [67] Abbott B P *et al* 2016 Sensitivity of the advanced LIGO detectors at the beginning of gravitational wave astronomy *Phys. Rev. D* **93** 112004
Abbott B P *et al* 2018 *Phys. Rev. D* **97** 059901 (addendum)
- [68] Ellis J, Lewicki M and No J M 2018 On the maximal strength of a first-order electroweak phase transition and its gravitational wave signal (arXiv:1809.08242)
- [69] Pedernales J S, Morley G W and Plenio M B 2019 Motional dynamical decoupling for matter-wave interferometry (arXiv:1906.00835)
- [70] Subramaniam C, Yamada T, Kobashi K, Sekiguchi A, Futaba D N, Yumura M and Hata K 2013 One hundred fold increase in current carrying capacity in a carbon nanotube–copper composite *Nat. Commun.* **4** 1–7
- [71] Fitzakerley D W *et al* 2016 Electron-cooled accumulation of 4×10^9 positrons for production and storage of antihydrogen atoms *J. Phys. B: At. Mol. Opt. Phys.* **49** 064001
- [72] Bose S and Morley G W 2018 Matter and spin superposition in vacuum experiment (massive) (arXiv:1810.07045)
- [73] Romero-Isart O 2011 Quantum superposition of massive objects and collapse models *Phys. Rev. A* **84** 052121
- [74] Bar-Gill N, Pham L M, Jarmola A, Budker D and Walsworth R L 2013 Solid-state electronic spin coherence time approaching one second *Nat. Commun.* **4** 1743
- [75] Aboeibeh M H, Cramer J, Bakker M A, Kalb N, Markham M, Twitche D J and Taminiau T H 2018 One-second coherence for a single electron spin coupled to a multi-qubit nuclear-spin environment *Nat. Commun.* **9** 2552
- [76] Knowles H S, Kara D M and Atatüre M 2014 Observing bulk diamond spin coherence in high-purity nanodiamonds *Nat. Mater.* **13** 21
- [77] Steane A M 2017 Matter-wave coherence limit owing to cosmic gravitational wave background *Phys. Lett. A* **381** 3905–8
- [78] Hughes S A and Thorne K S 1998 Seismic gravity-gradient noise in interferometric gravitational-wave detectors *Phys. Rev. D* **58** 122002
- [79] Moore C J, Cole R H and Berry C P L 2014 Gravitational-wave sensitivity curves *Class. Quantum Grav.* **32** 015014
- [80] Hogan J M, Hammer J, Chiow S-W, Dickerson S, Johnson D M S, Kovachy T, Sugarbaker A and Kasevich M A 2011 Precision angle sensor using an optical lever inside a Sagnac interferometer *Opt. Lett.* **36** 1698–700
- [81] Harms J, Slagmolen B J J, Adhikari R X, Miller M C, Evans M, Chen Y, Müller H and Ando M 2013 Low-frequency terrestrial gravitational-wave detectors *Phys. Rev. D* **88** 122003
- [82] Chaibi W, Geiger R, Canuel B, Bertoldi A, Landragin A and Bouyer P 2016 Low frequency gravitational wave detection with ground-based atom interferometer arrays *Phys. Rev. D* **93** 021101(R)
- [83] Harms J, DeSalvo R, Dorscher S and Mandic V 2009 Simulation of underground gravity gradients from stochastic seismic fields *Phys. Rev. D* **80** 122001
- [84] Saulson P R 1984 Terrestrial gravitational noise on a gravitational wave antenna *Phys. Rev. D* **30** 732
- [85] Pitkin M, Reid S, Rowan S and Hough J 2011 Gravitational wave detection by interferometry (ground and space) *Living Rev. Relativ.* **14** 5
- [86] Jan H 2015 Terrestrial gravity fluctuations *Living Rev. Relativ.* **18** 3
- [87] Nishida K 2017 Ambient seismic wave field *Proc. Jpn. Acad. B* **93** 423–48
- [88] Maher-McWilliams C, Douglas P and Barker P F 2012 Laser-driven acceleration of neutral particles *Nat. Photon.* **6** 386
- [89] Sugime H, Santiago E, Yang J, D’Arsié L, Oliver R A, Bhardwaj S, Cepek C and Robertson J 2013 Low temperature growth of ultra-high mass density carbon nanotube forests on conductive supports *Appl. Phys. Lett.* **103** 073116
- [90] Mourou G, Stancampiano C V and Blumenthal D 1981 Picosecond microwave pulse generation *Appl. Phys. Lett.* **38** 470–2
- [91] Kim J, Cox J A, Chen J and Kärtner F X 2008 Drift-free femtosecond timing synchronization of remote optical and microwave sources *Nat. Photon.* **2** 733–6
- [92] Ford L H 1998 Casimir force between a dielectric sphere and a wall: a model for amplification of vacuum fluctuations *Phys. Rev. A* **58** 4279–86
- [93] Speake C C and Trenkel C 2003 Forces between conducting surfaces due to spatial variations of surface potential *Phys. Rev. Lett.* **90** 160403
- [94] Nimmrichter S and Hornberger K 2013 Macroscopicity of mechanical quantum superposition states *Phys. Rev. Lett.* **110** 160403
- [95] Kovachy T, Asenbaum P, Overstreet C, Donnelly C A, Dickerson S M, Sugarbaker A, Hogan J M and Kasevich M A 2015 Quantum superposition at the half-metre scale *Nature* **528** 530
- [96] Nimmrichter S, Hornberger K, Haslinger P and Arndt M 2011 Testing spontaneous localization theories with matter-wave interferometry *Phys. Rev. A* **83** 043621
- [97] Biswas T, Gerwick E, Koivisto T and Mazumdar A 2012 Towards singularity and ghost free theories of gravity *Phys. Rev. Lett.* **108** 031101
- [98] Biswas T, Mazumdar A and Siegel W 2006 Bouncing universes in string-inspired gravity *J. Cosmol. Astropart. Phys.* **2006** 009
- [99] Buoninfante L, Lambiase G and Mazumdar A 2018 Quantum solitonic wave-packet of a meso-scopic system in singularity free gravity *Nucl. Phys. B* **931** 250–61
- [100] Buoninfante L, Lambiase G and Mazumdar A 2018 Quantum spreading of a self-gravitating wave-packet in singularity free gravity *Eur. Phys. J C* **78** 73